CrossMark

ARTICLE

Atomistic simulation of crack propagation in single crystal tungsten under cyclic loading

Xin-Tong Shu
College of Materials Science and Engineering, Hunan University, Changsha 410082, China
Shi-fang Xiao[a] and Hui-qiu Deng
Department of Applied Physics, School of Physics and Electronics, Hunan University, Changsha 410082, China
Lei Ma
College of Physics and Electronic Science, Hunan University of Arts and Science, Changde 415000, China
Wangyu Hu[b]
College of Materials Science and Engineering, Hunan University, Changsha 410082, China

(Received 23 December 2016; accepted 13 March 2017)

The propagation of a pre-existing center crack in single crystal tungsten under cyclic loading was examined by molecular dynamics (MD) simulations at various temperatures. The results indicated that the deformation mechanism and fracture behavior at crack tip were differences for variously oriented cracks. The [001](010) crack propagated as the form of the formation of slip, while the deformation mechanisms of [10−1](101) crack were blunting voids at 300 K. At higher temperature, many more slip systems were activated resulting in the change of mode of crack propagation. Simulated results showed that the effect of temperature on deformation mechanism and fracture behavior of [001](010) crack was more sensitive than that of [10−1](101) crack. Meanwhile, the influence of a $5\langle 310\rangle\{110\}$ model grain boundary (GB) on crack propagation was also discussed. Detailed analysis showed that the grain boundary resisted the crack growth by changing the deformation mechanisms and the path of crack propagation at crack tip before the crack reached the grain boundary, and had an important influence on the crack growth rate.

I. INTRODUCTION

Tungsten is remarkable for its robustness, high heat conductivity, and low sputtering erosion, and it has the highest melting point for all the nonalloyed metals. Due to the above advantages, tungsten becomes one of the important candidates of the plasma facing materials (PFM), and is most probable to be used as the first wall material in the future fusion reactor. The properties of tungsten, such as recrystallization behavior, the ductile-to-brittle transition and thermal stability, have been investigated experimentally and theoretically.[1–6] However, the study on the fatigue crack growth in tungsten is still rather poor. As PFM, tungsten is supposed to bear high thermal loads, which could induce high thermal stresses and the formation of crack. The crack propagation in tungsten will cause the fatal destruction of the components. Therefore, it is important to understand the fracture mechanisms of tungsten due to the crack propagation.

Recently, the fatigue crack extension behavior has been widely discussed by molecular dynamics (MD) simulations. Much research shows that the crack propagation and dislocation emission are influenced by the crack orientation.[7–11] In addition, there are many other factors influencing the mode of crack growth. Lee et al.[12] analyzed the influence of grain boundary property variation on rupture resistance of poly-crystalline tungsten. The results showed that the change of 10% in GB fracture energy caused significantly different crack patterns with different main crack extension direction and the density of microcracks. And, grain boundaries play an important role in crack propagation, Ma[13] have examined the effect of $\sum 3$ and $\sum 5$ on crack growth in bcc iron under cyclic loading, and found that $\sum 3$ caused the brittle fracture, while $\sum 5$ resisted crack extension. Besides, the loading pattern had a significant effect on the behavior of fatigue crack growth,[14,15] and void coalescence is an important damage mechanism at crack tip. Therefore, the study of the nucleation and growth of voids in ductile metals is significant for understanding of the fatigue failure. Zhao[16] discussed cylindrical nano-void growth in single crystal copper, and investigated the influence of the cell size, crystal orientation and original void volume fraction on the macroscopic stress–strain curve and incipient yield strength. Their results suggested that cell size had great effects on the incipient yield strength for a given void volume fraction.

Contributing Editor: Susan B. Sinnott
Address all correspondence to these authors.
[a]e-mail: shifangxiao@hnu.edu.cn
[b]e-mail: wyuhu@hnu.edu.cn
DOI: 10.1557/jmr.2017.114

 © Materials Research Society 2017

https://doi.org/10.1557/jmr.2017.114 Published online by Cambridge University Press

Though MD simulation is widely used in fatigue crack propagation, the research of fatigue crack growth in tungsten is still poor. To discuss the influence of the anisotropic microstructure on the fracture toughness and brittle–ductile transition in tungsten, Ermile et al.[17] extracted longitudinal, radial, and circumferential specimens. Their studies found that the microstructure of polycrystalline tungsten played a notable role in crack propagation mechanism. Longitudinal specimens failed by predominantly intergranular fracture up to 800 K, whereas transgranular cleavage was observed at low test temperatures for radial and circumferentially oriented specimens. In addition, Yu et al.[18] investigated the influence of hydrogen on the crack growth behavior in pre-cracked tungsten single-crystals, and the results showed that hydrogen could either enhance or reduce the ductility of tungsten. On one hand, high hydrogen concentration could lead to the rearrangement of tungsten atoms at crack front and facilitate the dislocation emission from the crack tip, which would delay the crack propagation. On the other hand, a void could be nucleated in a local hydrogen-rich area, which accelerated the crack propagation.

In this paper, we mainly focus on investigating the crack propagation path, microscopic deformation mechanism and failure mechanism in tungsten by analyzing microstructure evolution around the crack front under cyclic loading at different temperature. Besides, the $\sum 5$ grain boundary models are constructed to discuss the effect of GB on the behavior of crack growth in tungsten. Finally, the crack growth rate is discussed by the variation of crack length.

II. MODELING DETAILS AND INTERATOMIC POTENTIAL

A. Modeling details

The crack model with a pre-existing center crack was constructed by removing some atoms in single crystal tungsten as shown in Fig. 1(a). The sizes of model were $150a \times 150a \times 40a$ in the x, y, and z directions, the length of initial crack was equal to $10a$ and its width was $2a$, where a was the lattice constant of tungsten. The [001](010) crack and [10−1](101) crack were constructed, where (010) and (101) represent initial crack face, [001] and [10−1] represent the orientation of initial crack front. The loading were applied in [010] and [101] direction, respectively. Periodic boundary conditions were applied to x and z directions, and the free boundary condition was applied in y direction. In the MD simulations, the constant strain rate was 1×10^9 s^{-1}. The strain cyclic loading was applied in y axis with increasing

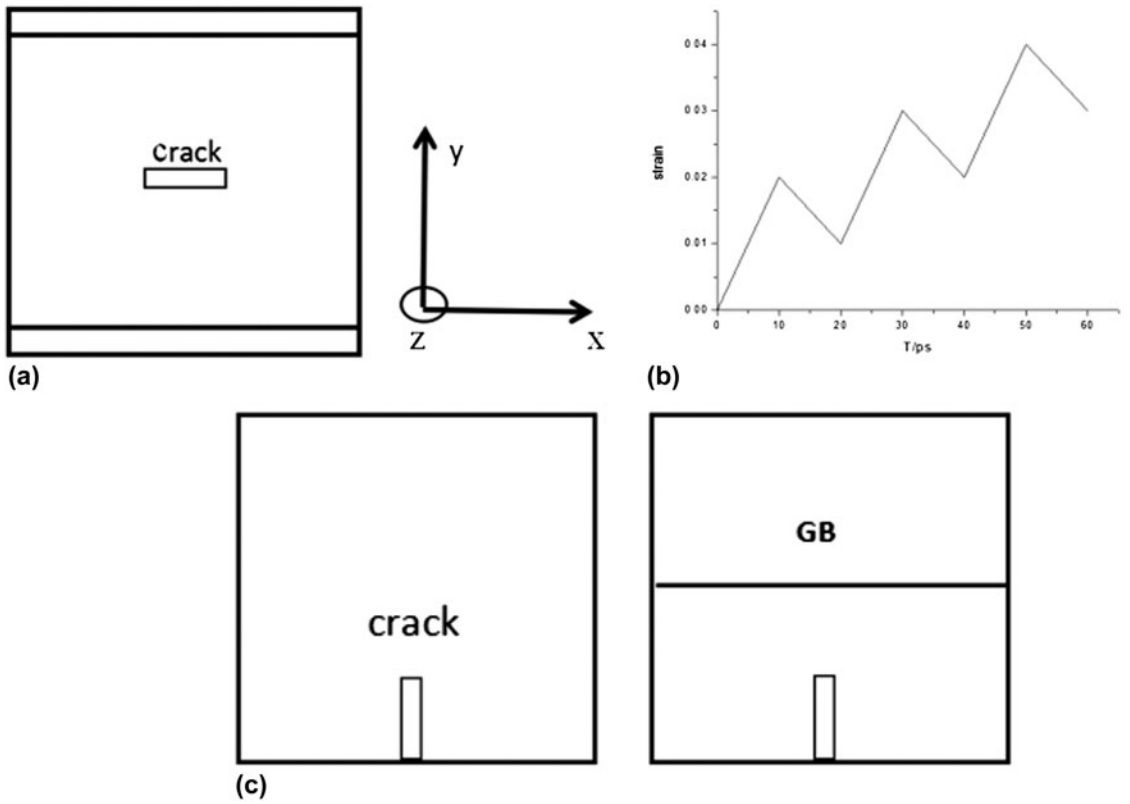


FIG. 1. Schematic illustration of initial crack models and the pattern of cyclic loading in tungsten: (a) a pre-existing center crack model, (b) the pattern of cyclic loading, and (c) containing a grain boundary model.

https://doi.org/10.1557/jmr.2017.114 Published online by Cambridge University Press

strain amplitude. The initial constant strain amplitude of cyclic loading was 0.02 and the unloading ratio was 50%, which was illustrated in Fig. 1(b). Before cyclic loading, the crack models were relaxed by running 20 ps with a time step of 1 fs until the systems were equilibration and then were cyclically loaded. The number of cyclic loading for all the crack models ranged from 1 to 30. Furthermore, to discuss the effect of GB on fatigue crack growth behavior, a sample containing a $\sum 5$ was constructed as sketched in Fig. 1(c). The strain cyclic loading was added in x axis with increasing strain amplitude. In these models, the free boundary condition was applied in y direction to stop the crack central vacancy from filling with ghost from the adjacent cells.[19]

B. Interatomic potential

The embedded atom method (EAM) potential was adopted in MD simulations, which was constructed by Ackland et al.,[20] and the form of this potential was given out by Han et al.[21] Before performing the simulation, the fundamental lattice properties of this potential were calculated by the Large-scale Atomic/Molecular Massively Parallel Simulation (LAMMPS)[22] code, such as elastic constant, lattice constant, vacancy formation energy, and binding energy as shown in Table I, that agreed well with experimental values.[23–26] Meanwhile, the mechanical properties of this potential were also verified. Figure 2 showed relative energy difference of {100}, {111}, {112} with {110} surface. As shown, the calculated values of relative energy difference agreed well with other reference values.[27] More importantly, all potentials calculated {110} surface energy was the lowest, and specific values were presented in Table II. Although our values are less than experimental data,[28] it was consistent with other reference values within 6% error range. Furthermore, the stacking fault energy of ⟨111⟩ {112} system was calculated. The maximum stacking fault energy was 2136 mJ/m^2, that agreed well with the values of 2089, 2181, and 2346 mJ/m^2 calculated by the potentials of KLL, JO, and FOI.[27] But a little bigger than the values of DFT and ZWJ[27] that correspond to 1760 and 1997 mJ/m^2, respectively.

To understand the fracture behavior of single crystal tungsten under monotonic tensile along the [0 1 0] direction, we construct a model with the same size as [001](010) crack model but no crack. In addition, the constant strain rate of 1×10^9 s^{-1} and room temperature were used for this simulation. The results and other calculations were presented in Table III. The peak stress in the [0 1 0] direction was 38.7 GPa in this work, that agreed well with the values of 36.3 and 36.9 GPa obtained from W-BHS and W-PADE,[29,30] respectively. But it had relatively large deviation from the reference value of 26.96, 29.1, and 61 GPa calculated by Chen et al.,[31] Liu et al.[32] and Kelly,[33] respectively. Moreover, the strain corresponding to maximum stress varied from 7.1% to 25%. Because all of the above values were estimated, so there was inevitable deviation. Based on the above test results, we could use this potential to simulate fatigue fracture behavior of single crystal tungsten. The following simulations were conducted by LAMMPS code, and the microstructure evolution was visualized by OVITIO,[34] analyzed with the common neighbor analysis (CNA).[35]

TABLE I. The fundamental lattice properties of tungsten single crystals.

Lattice (Å)	E_{coh} (eV)	E^f_v (eV)	C_{11} (GPa)	C_{12} (GPa)	C_{44} (GPa)
3.1652	8.91	3.67	533	205	163
3.165[23]	8.9[23]	3.1–4.0[24,25]	501–521[26]	199–207[26]	151–160[26]

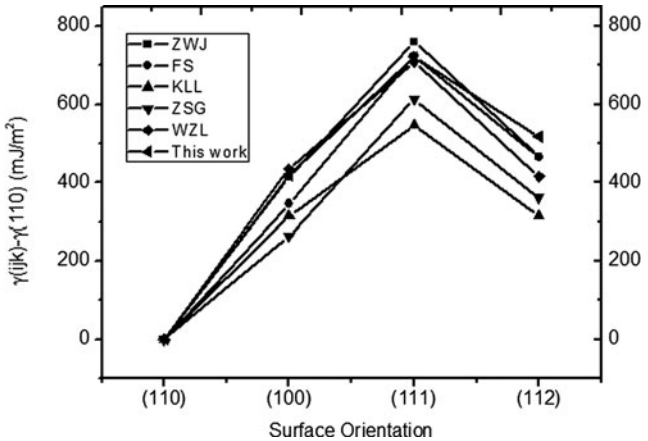


FIG. 2. Relative energy difference of {100}, {111}, {112}, with {110} surface.

TABLE II. The specific values of (110) free surface energy.

(mJ/m^2)	ZWJ	FS	WZL	KLL	ZSG	This work	Exp.[28]
γ_{110}	2566	2575	2402	2435	2629	2553	3250

TABLE III. The ideal tensile strength σ_m (GPa) and corresponding strain ε_m from our and other calculations in the [1 0 0] direction.

	σ_m (GPa)	ε_m (%)
This work	38.7	7.2
W-PADE[29,30]	36.9	11.7
W-BHS[29,30]	36.3	11.5
Chen et al.[31]	26.96	9.5
Liu et al.[32]	29.1	14
Kelly and Macmillan[33]	61	25

https://doi.org/10.1557/jmr.2017.114 Published online by Cambridge University Press

III. RESULT AND DISCUSSION

A. The microstructure evolution of [001](010) crack

Figure 3 showed the process of evolution mechanisms of microstructures analyzed by CNA for [001](010) crack during cycle loading at 300 K. At cycle 4, the slip bands were observed at crack tip, which is caused by the stress concentration at crack tip, and the slip direction along the [110] directions. As the loading increased, the stress concentration was intense at crack tip, and the local slip bands extended around the crack tip at cycle 5. During this time, the peak stress calculated for the entirely cyclic loading process was 29.74 GPa and corresponding strain was 4.51%. The threshold stress intensity factor K_I was obtained from the Griffith level $K_I = \sigma(\pi a)^{0.5}$, where σ is equal to 29.74 GPa and a is the crack length. In the present work, the K_I was 2.97 MPa $\sqrt{m}$, which was in good agreement with the experimental value of 3–3.5 MPa $\sqrt{m}$ measured by Gludovatz et al. in the technically pure tungsten (W > 99.97%).[36] Up to the 6th cycle, the crack initiation arise in {110} planes and the value of Schmidt factor was equal to 0.408 this moment. This is in agreement with experimental observations that cleavage on the {110} planes in single crystal tungsten under tensile tests.[37] At cycle 7, the crack length increased fast along {111} direction. Moreover, the cross slip band was also observed around crack tip, which was similar to the finding in bcc iron.[13] Before the cycle 8, the crack showed ductile rupture and the deformation mechanisms mainly manifested slip at crack tip. When the loading was further increasing, the crack grew as the form of void nucleation, void extension, and link. So the crack growth entered into the rapidly extending stage in cycle 8 and 9. From cycle 8 to cycle 9, the dominant deformation mechanism was void nucleation, and the crack showed brittleness advance. Figure 4 presented the deformation characteristic of crack tip and the evolution process of crack propagation path. In Fig. 4(a), the main deformation mechanism was the slip band at crack tip, and the slip direction was along ⟨110⟩ direction. Subsequently, the crack propagated presented ductile rupture, and the dominant deformation mechanism was also slip around crack tip, which was presented in Fig. 4(b). In Fig. 4(c), the deformation mechanism changed, it mainly showed void nucleation at crack tip. Based on the above analysis, the crack propagation path could be decomposed into the following parts. Firstly, the crack showed ductile rupture

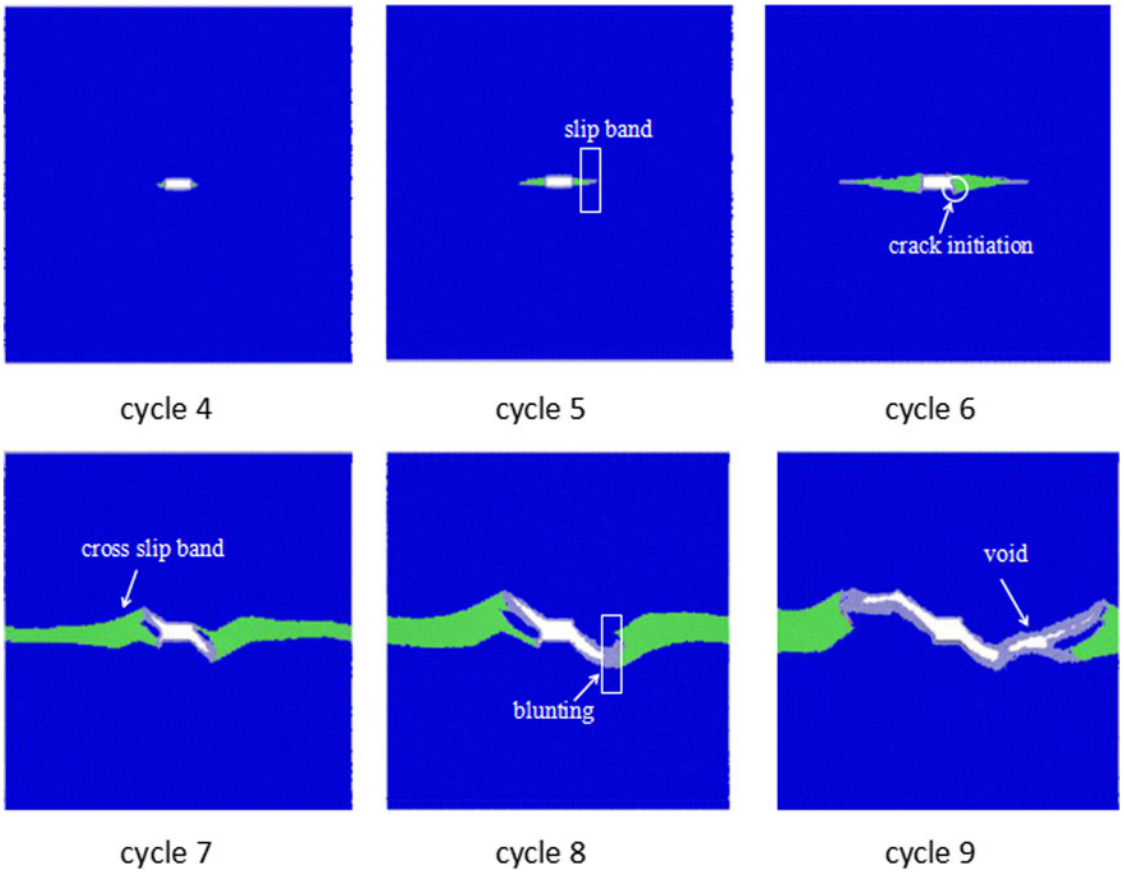


FIG. 3. The microstructure evolution analyzed by CNA on crack propagation for [001](010) crack in single crystal tungsten, the blue stand for bcc tungsten structure and green stand for fcc slip band structure.

https://doi.org/10.1557/jmr.2017.114 Published online by Cambridge University Press

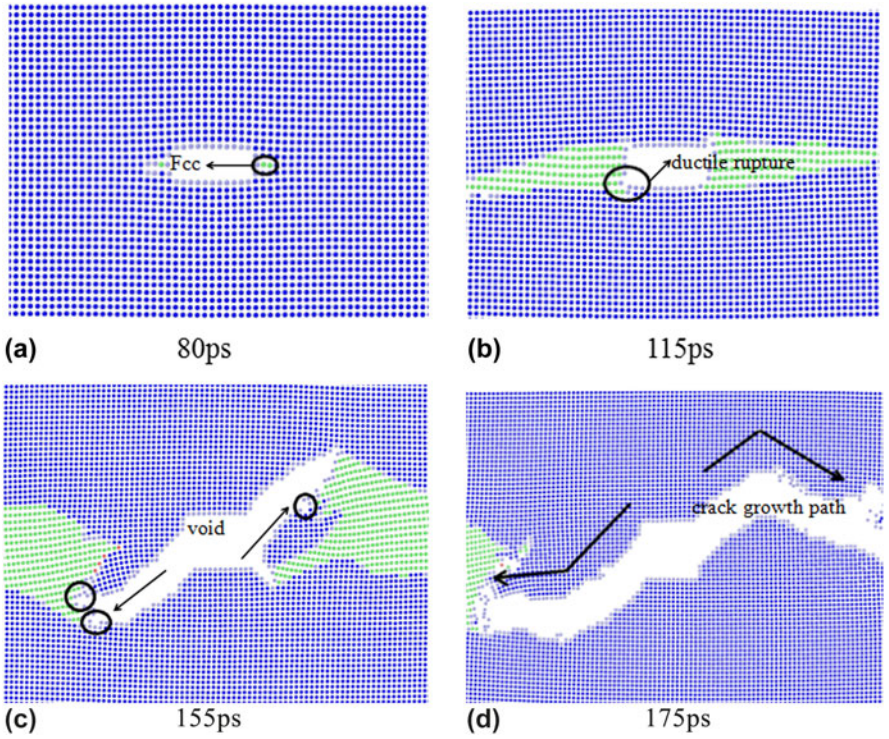


FIG. 4. Geometry of the deformation mechanism of crack growth and the evolution process of crack propagation path at (a) 80ps, (b) 115ps, (c) 155ps, and (d) 175ps.

and the crack propagation path inclined to original crack plane at an angle of 45°. Next, the stress concentration was relaxed due to the formation of sip bands at crack tip, which inhibited the crack growth. Finally, the void nucleated and linked up with the original crack, which resulted in the changes of crack growth path as shown in Fig. 4(d). The similar path of crack propagation was observed experimentally.[36]

Figure 5 presented the microstructure evolution for [001](010) crack at 600 and 900 K. At a temperature of 600 K, more slip systems were activated and the blunt phenomenon was not significant as shown in Fig. 5(a). The maximum stress calculated under this temperature condition was 26.38 GPa and corresponding strain was 4.60%. As the temperature further increased, the plastic region broadened caused by more and more activated slip systems at cycle 6, which could be seen in Fig. 5(b). From cycle 8 to cycle 11, the crack expanded in double {110} planes due to more slip systems. During the whole process, crack propagation was in the form of ductile rupture, and the mechanisms of deformation mainly were slip and blunting. To further analyze the effect of temperature on fracture behavior, the maximum stress was also calculated under cyclic loading at 900 K as shown in Table IV. Usually, the stress–strain curve could be divided into four stages: elastic, plastic, damage, and failure stages. To better explain the effect of temperature on fracture behavior of single crystal tungsten, we calculated the strain of second stages (plastic). In the present work, the second stage was defined as the range from the peak stress to the lowest point of a sharp stress drop.[33] The results of maximum stress and various strain were shown in Table IV, where ε_k represented the strain of the lowest point in second stages of stress–strain curve. Based on the values of Table IV, we could have a conclusion that the plastic range became larger with the increase of temperature for [001](010) crack attributed to the activation of more slip systems in single crystal tungsten. What's more, the plastic range at 900 K was almost twice as large as that of 300 K. In short, the temperature had a great influence on fracture behavior of [001](010) crack growth, and the ductility at elevated temperature was obviously higher than that at room temperature.

B. [10-1](101) crack propagation behavior

In this section, we simulated the deformation and fracture characteristics of [10−1](101) crack in single crystal tungsten at 300, 600, and 900 K. Figure 6(a) showed the evolution process of [10−1](101) crack in tungsten at 300 K. During the entire cyclic loading process, the peak stress was 27.66 GPa and corresponding strain was 5.6% as shown in Table IV. While the range between ε_m and ε_k was equal to 0.75%, which is much less than that of the [001](010) crack. The main reason for this difference was that the mechanisms of deformation and fracture behavior at crack tip changed. From cycle 7 to 8, the blunting was appeared at crack front due to the intense stress concentration. The plastic

https://doi.org/10.1557/jmr.2017.114 Published online by Cambridge University Press

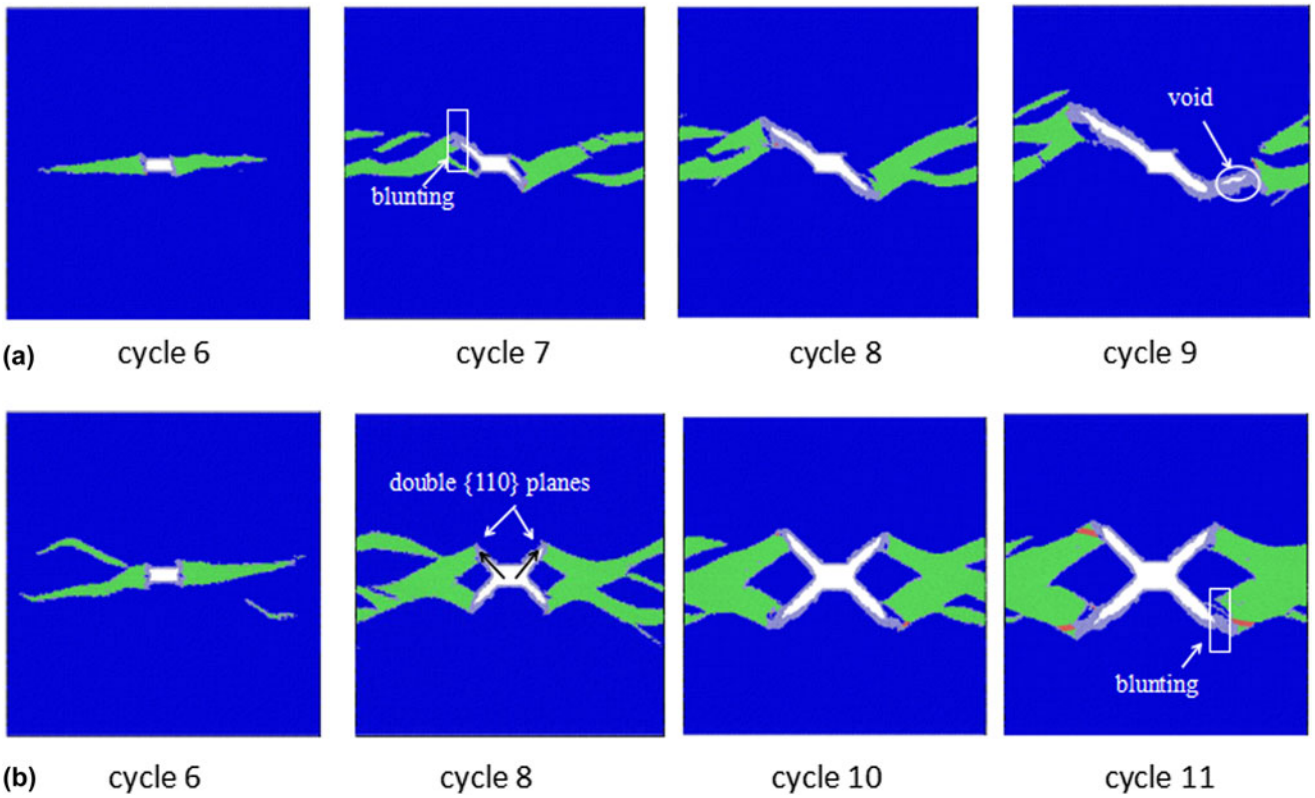


FIG. 5. The microstructure evolution analyzed by CNA on crack propagation for [001](010) crack in single crystal tungsten at (a) 600 K and (b) 900 K. The blue stands for bcc tungsten structure, green stands for fcc slip band structure and red stands for hcp structure.

TABLE IV. The peak stress, ε_m and ε_k for all models at different temperature.

Crack model	σ_m (GPa)	ε_m (%)	ε_k (%)	$\varepsilon_k - \varepsilon_m$ (%)
300 K, [001](010)	29.74	4.51	6.79	2.28
600 K, [001](010)	26.38	4.60	7.58	2.98
900 K, [001](010)	24.47	4.83	9.37	4.54
300 K, [101](101)	27.66	5.60	6.32	0.72
600 K, [101](101)	25.97	5.63	6.48	0.85
900 K, [101](101)	25.09	5.67	6.65	0.98

zone of crack tip was also formed near the crack tip. In addition, the fcc and hcp slip bands were also observed, which was induced by the movement of dislocations around the crack tip. When the loading was further increasing, the blunting extended and void nucleation formed in the front of the crack tip at cycle 9, and the crack showed brittleness propagation. With the increasing of temperature, the plastic deformation zone was more obvious. But the values of ε_k were almost unchanged, corresponding to 6.48% and 6.45%, respectively. Which indicated that the temperature had little effect on fracture behavior of [10−1](101) crack in single crystal tungsten, and the crack also showed the brittleness extension as observed in Figs. 6(b) and 6(c). Comparing [001](010) crack with [10−1](101) crack, we could draw the conclusion that the effect of temperature on deformation mechanism and fracture behavior of [001](010) crack was more significant than that of the latter.

C. Effect of grain boundary and temperature on crack growth

Grain boundaries generally act as dislocation obstacles, sinks, and sources in fatigue crack propagation behavior. When the stress exceeded a critical value of dislocation pileup, the material either yielded by transmission of slip to the neighboring grain or initiated microcrack at the boundary,[38,39] which depended on intrinsic material properties and on extrinsic factors such as the distribution of atom stresses, strain rate, or temperature. Wang et al.[40] investigated the effects of grain size on the mechanical behavior of nano-polycrystal alpha-Fe under uniaxial tensile loading. Their found crack nucleated at the intersections of grain boundaries due to the stress to concentrate there. In this part, the $\sum 5$ GB model was constructed to study the effect of GB on crack propagation at 5 and 100 K, and an additional model without grain boundary was also simulated at 5 K for comparison.

Figure 7(a) showed the fatigue crack growth for the no-grain boundary model from cycle 10 to 20. The result indicated that the dislocations emit along ⟨111⟩ direction, and the slip band was formed at crack tip due to the

https://doi.org/10.1557/jmr.2017.114 Published online by Cambridge University Press

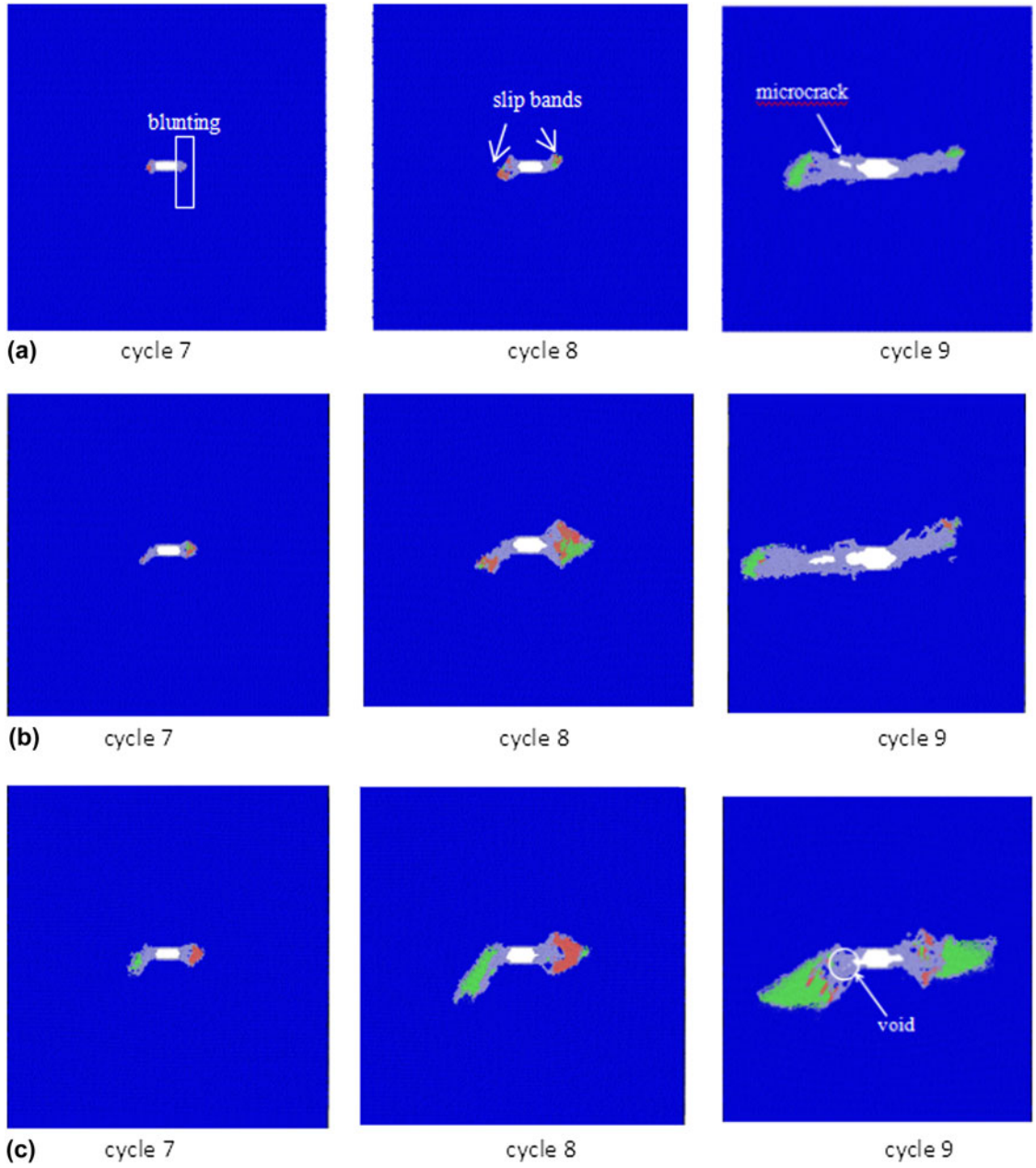


FIG. 6. The microstructure evolution analyzed by CNA on crack propagation for [10−1](101) crack in single crystal tungsten at (a) 300 K, (b) 600 K, and (c) 900 K. The blue stands for bcc tungsten structure, green stands for fcc slip band structure, and red stands for hcp structure.

dislocation motion. When the loading increased, the crack expanded along ⟨111⟩ direction and showed ductile fracture before cycle 21. Up to cycle 21, the main deformation mechanisms were voids nucleation, and the crack presented brittleness fracture. Figure 7(b) showed the effect of $\sum 5$ grain boundary on crack growth at 5 K. One can see that before cycle 10, there was no obvious difference from the no-grain boundary crack model. For the no-grain boundary crack model, up to cycle 17, the crack kept ductile fracture due to the release of stress caused by the extension and movement of slip bands at crack tip as shown in Fig. 7(a). But for the grain boundary crack model, due to the appearance of grain boundaries, the movement of the slip bands was blocked so that the stress concentration at crack tip was not be released, the crack propagated by voids nucleation as shown in the Fig. 7(b). At cycle 18, the crack grew to the grain boundaries. From cycle 18 to 20, the crack has no extension due to the appearance of grain boundaries. With the loading increasing, the secondary voids nucleated in the upper of grain boundaries and linked with the crack tip at cycle 21, which caused the change of crack

https://doi.org/10.1557/jmr.2017.114 Published online by Cambridge University Press

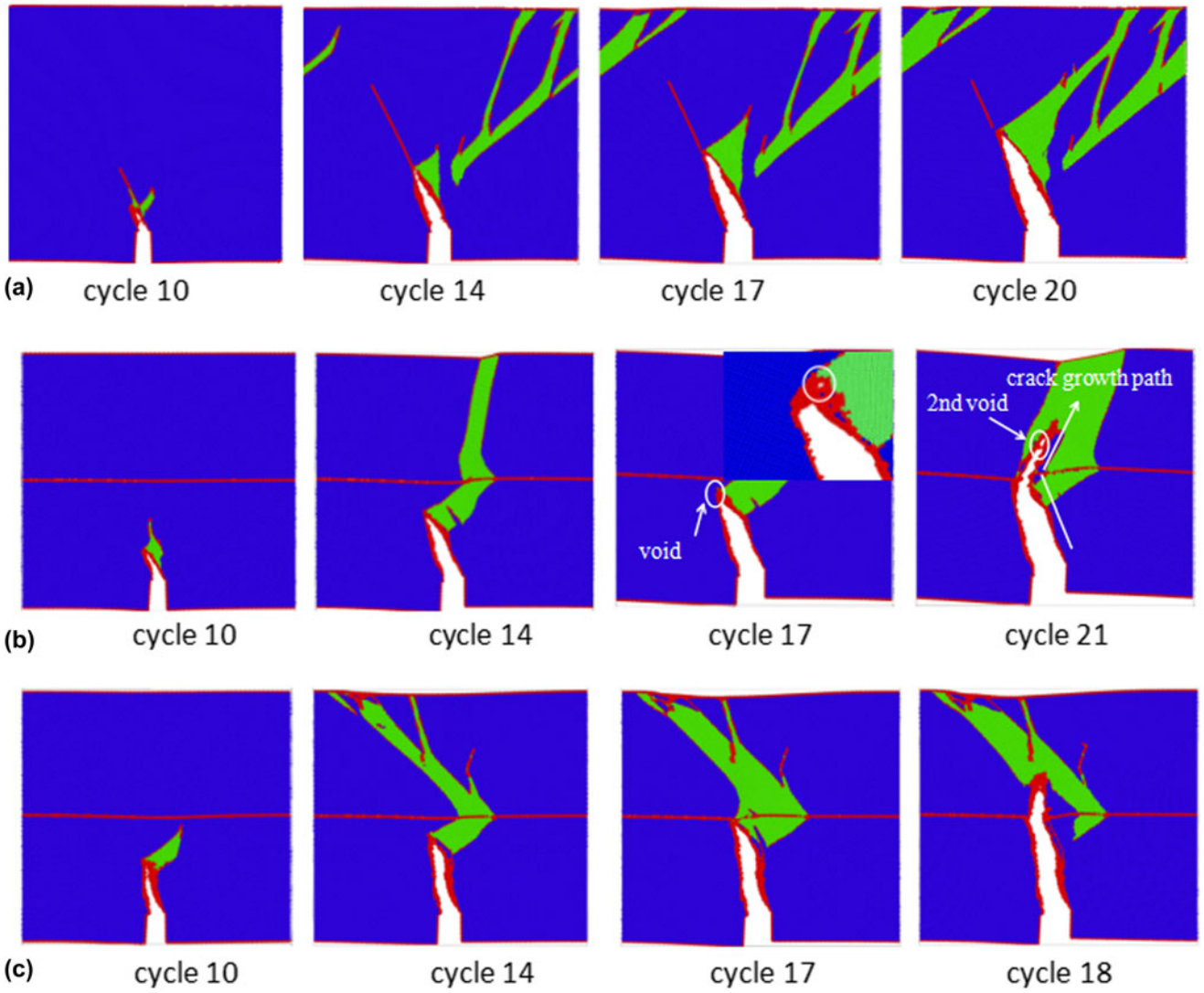


FIG. 7. The time evolution of crack growth (a) for nongrain boundary at 5 K, (b) for grain boundary at 5 K, and (c) for grain boundary at 100 K.

propagation path. Similar to the above crack propagation process another process was reported experimentally by Yan and Fan in 2524 aluminum alloy.[41] In their experiments, the change of the main crack propagation direction after it passed through the GB and continued to expand by linked with the microcracks ahead of the crack tip were observed. Figure 7(c) showed the simulated results of $\sum 5$ grain boundary models at 100 K. Before cycle 18, there was no obvious difference on crack growth behavior from that at the temperature of 5 K. But at cycle 18, the crack passed through grain boundary and the obvious obstacles was not found. In summary, grain boundary resisted the crack growth before the crack reached near the grain boundary, while it was conducive to the nucleation of the secondary voids after the crack reached the grain boundary and changed the path of crack propagation. In addition, higher temperature favored voids nucleation, which resulted in the crack passing through grain boundary quickly.

D. Crack growth rate

The variation of crack length with the number of cycles under cyclic loading was calculated. Figure 8(a) showed the crack growth rate of [001](010) and [10−1](101) cracks in single crystal tungsten at 300 K. The results showed that the [001](010) crack propagated relatively slow from cycle 6 to cycle 8. After cycle 8, the crack propagated rapidly due to the formation of void, so the crack growth rate increased as shown in Fig. 8(a). The [10−1](101) crack showed blunting phenomenon from cycle 6 to 8, therefore, the crack growth rate was very small. Subsequently, it increased rapidly due to the formation of voids. Figure 8(b) revealed the variation of

https://doi.org/10.1557/jmr.2017.114 Published online by Cambridge University Press

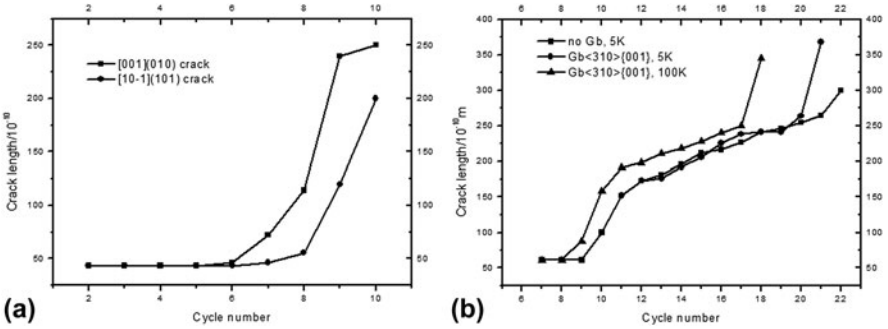


FIG. 8. Crack growth rate (a) for different orientations and (b) for different models.

crack length of $\sum5\langle310\rangle\{110\}$ crack models and $\langle310\rangle\{110\}$ crack models. The results showed that there was similar trend about crack growth behavior in $\sum5\langle310\rangle\{110\}$ crack models and $\langle310\rangle\{110\}$ crack models before cycle 15 at 5 K. During cycle 15 to 18, the crack growth rate of $\sum5\langle310\rangle\{110\}$ crack models was larger than $\langle310\rangle\{110\}$ crack models. This was mostly because the $\sum5$ GB hindered the movement of slip bands so that stress concentration was intense at crack tip, and then the voids appeared at crack tip, and the crack extended rapidly. From cycle 18 to 19, due to the absence of grain boundary, the growth rate of $\sum5\langle310\rangle\{110\}$ crack models was smaller than that of $\langle310\rangle\{110\}$ crack models. After cycle 19, the voids appeared over the grain boundary, so the crack extended rapidly again as shown in Fig. 8(b).

IV. CONCLUSION

In this study, we have performed the MD simulation to examine fatigue fracture mechanical behaviors of [001](010) and [10−1](101) crack at the temperature of 300, 600, and 900 K under cyclic loading in single tungsten. In [001](010) crack model at 300 K, the $\langle111\rangle\{110\}$ slip system and slip band were observed in crack tip before cycle 8. During this period, the crack propagation showed ductile cracking. After cycle 8, the dominant deformation mechanism was void nucleation. So crack propagation showed brittleness. At higher temperature, crack propagation was in the form of ductile rupture, and the mechanisms of deformation were slip and blunting due to more slip systems activated. But for [10−1](101) crack, the deformed mechanism was blunt and void nucleation. Therefore, crack propagation showed brittleness. Meanwhile, we constructed the $\langle310\rangle\{001\}$ crack model and explored the effect of $\sum5$ grain boundary and temperature on fatigue fracture mechanical behaviors. The results showed that the grain boundary resisted the crack growth before the crack reached the grain boundary, while it was conducive to the nucleation of the secondary voids after the crack reached the grain boundary and changed the path of crack propagation. In addition, higher temperature favored voids nucleation, which resulted in the crack passing through grain boundary quickly.

ACKNOWLEDGMENTS

This work is supported by the National Magnetic Confinement Fusion Science Program of China (Grant No. 2014GB104002), the National Natural Science Foundation of China (Grant No. U1530151, 51471068), and the Specialized Research Fund for the Doctoral Program of Higher Education of China (Grant No. 20120161110015). We also appreciate the support by Atomic Simulation Lab of Hunan University and the computation platform of National Supper-Computer Center in Changsha.

REFERENCES

1. Y. Cheng, M. Mrovec, and P. Gumbsch: Crack nucleation at the Σ9(221) symmetrical tilt grain boundary in tungsten. *Mater. Sci. Eng., A* **483**(4), 329 (2008).
2. Y. Zhang, A.V. Ganeev, J.T. Wang, J.Q. Liu, and I.V. Alexandrov: Observations on the ductile-to-brittle transition in ultrafine-grained tungsten of commercial purity. *Mater. Sci. Eng., A* **503**, 37 (2009).
3. S.N. Mathaudhu, A.J. deRosset, K.T. Hartwig, and L.J. Kecskes: Microstructures and recrystallization behavior of severely hot-deformed tungsten. *Mater. Sci. Eng., A* **503**, 28 (2009).
4. A. Alfonso, D. Juul Jensen, G.N. Luo, and W. Pantleon: Recrystallization kinetics of warm-rolled tungsten in the temperature range 1150–1350 °C. *J. Nucl. Mater.* **455**, 591 (2014).
5. A. Alfonso, D. Juul Jensen, G.N. Luo, and W. Pantleon: Thermal stability of a highly-deformed warm-rolled tungsten plate in the temperature range 1100–1250 °C. *Fusion Eng. Des.* **98–99**, 1924 (2015).
6. X.Y. Tan, L.M. Luo, Z.L. Lu, G.N. Luo, X. Zan, J.G. Cheng, and Y.C. Wu: Development of tungsten as plasma-facing materials by doping tantalum carbide nanoparticles. *Powder Technol.* **269**, 437 (2015).
7. G.P. Potirniche, J.L. Hearndon, M.F. Horstemeyer, and X.W. Ling: Lattice orientation effects on void growth and coalescence in fcc single crystals. *Int. J. Plast.* **22**(5), 921 (2006).
8. Y.F. Guo and D.L. Zhao: Atomistic simulation of structure evolution at a crack tip in bcc-iron. *Mater. Sci. Eng.* **448**(1–2), 281 (2007).
9. T. Tang, S. Kim, and M.F. Horstemeyer: Fatigue crack growth in magnesium single crystals under cyclic loading: Molecular dynamics simulation. *Comput. Mater. Sci.* **48**(2), 426 (2010).
10. H. Xie, T. Yu, F. Yin, and C. Tang: The effects of crack orientation on the twin formation from the crack tip in γ-Ni_3Al. *Mater. Sci. Eng., A* **580**, 99 (2013).

https://doi.org/10.1557/jmr.2017.114 Published online by Cambridge University Press

11. L. Ma, S.F. Xiao, H.Q. Deng, and W.Y. Hu: Atomic simulation of fatigue crack propagation in Ni_3Al. *Appl. Phys. A* **118**, 1399 (2015).
12. H. Lee and V. Tomar: Understanding effect of grain boundaries in the fracture behavior of polycrystalline tungsten under mode-I loading. *J. Eng. Mater. Technol.* **134**(3), 031010 (2012).
13. L. Ma, S.F. Xiao, H.Q. Deng, and W.Y. Hu: Molecular dynamics simulation of fatigue crack propagation in bcc iron under cyclic loading. *Int. J. Fatigue* **68**, 253 (2014).
14. G.P. Potirniche, M.F. Horstemeyer, B. Jelinek, and G.J. Wagner: Fatigue damage in nickel and copper single crystals at nanoscale. *Int. J. Fatigue* **27**, 1179 (2005).
15. A. Machová, J. Pokluda, A. Uhnáková, and P. Hora: 3D atomistic studies of fatigue behaviour of edge crack (001) in bcc iron loaded in mode I and II. *Int. J. Fatigue* **66**, 11 (2014).
16. K.J. Zhao, C.Q. Chen, Y.P. Shen, and T.J. Lu: Molecular dynamics study on the nano-void growth in face-centered cubic single crystal copper. *Comput. Mater. Sci.* **46**(3), 749 (2009).
17. E. Gaganidze, D. Rupp, and J. Aktaa: Fracture behaviour of polycrystalline tungsten. *J. Nucl. Mater.* **446**(s1–3), 240 (2014).
18. X. Yu, F. Gou, B. Li, and N. Zhang: Numerical study of the effect of hydrogen on the crack propagation behavior of single crystal tungsten. *Fusion Eng. Des.* **89**, 1096 (2014).
19. Y. Zhang, F.C. Zhang, L.H. Qian, and T.S. Wang: Atomic-scale simulation of iron phase boundary affecting crack propagation using molecular dynamics method. *Comput. Mater. Sci.* **50**(5), 1754 (2011).
20. Online source: National Institute of Standards and Technology: 2017. Available at: http://www.ctcms.nist.gov/potentials/ (accessed 05 March 2016).
21. S. Han, L.A. Zepeda-Ruiz, G.J. Ackland, R. Car, and D.J. Srolovitz: Interatomic potential for vanadium suitable for radiation damage simulations. *J. Appl. Phys.* **93**(6), 3328 (2003).
22. S. Plimpton: Fast parallel algorithms for short-range molecular dynamics. *J. Comput. Phys.* **117**, 1 (1995).
23. C. Kittel: *Introduction to Solid State Physics*, 7th ed. (Wiley Press, New York, 1996); p. 57.
24. K. Maier, M. Peo, B. Saile, H.E. Schaefer, and A. Seeger: High-temperature positron annihilation and vacancy formation in refractory metals. *Philos. Mag. A* **40**, 701 (1979).
25. H.J. Wollenberger: Point defects. *Phys. Metall.* **2**, 1139 (1983).
26. D.I. Bolef and J. De Klerk: Elastic constants of single-crystal Mo and W between 77° and 500° K. *J. Appl. Phys.* **33**(7), 2311 (1962).
27. G. Bonny, D. Terentyev, A. Bakaev, P. Grigorev, and D. Van Neck: Many-body central force potentials for tungsten. *Modell. Simul. Mater. Sci. Eng.* **22**(22), 053001 (2014).
28. W.R. Tyson and W.A. Miller: Surface free energies of solid metals: Estimation from liquid surface tension measurements. *Surf. Sci.* **62**(1), 267 (1977).
29. G.B. Bachelet, D.R. Hamann, and M. Schluter: Pseudopotentials that work: From H to Pu. *Phys. Rev. B: Condens. Matter Mater. Phys.* **26**, 4199 (1982).
30. S. Giusepponi and M. Celino: The ideal tensile strength of tungsten and tungsten alloys by first-principles calculations. *J. Nucl. Mater.* **435**, 52 (2013).
31. Z. Chen, L.J. Kecskes, K. Zhu, and Q. Wei: Atomistic simulations of the effect of embedded hydrogen and helium on the tensile properties of monocrystalline and nanocrystalline tungsten. *J. Nucl. Mater.* **481**, 190 (2016).
32. Y.L. Liu, H.B. Zhou, Y. Zhang, S. Jin, and G.H. Lu: The ideal tensile strength and deformation behavior of a tungsten single crystal. *Nucl. Instrum. Methods Phys. Res.* **267**(18), 3282 (2009).
33. A. Kelly and N.H. Macmillan: *Strong Solids*, Vol. **1015**, 3rd ed. (Clarendon Press, Oxford, 1986).
34. A. Stukowski: Visualization and analysis of atomistic simulation data with OVITO–the open visualization tool. *Modell. Simul. Mater. Sci. Eng.* **18**(1), 015012 (2010).
35. J.D. Honeycutt and H.C. Andersen: Molecular dynamics study of melting and freezing of small Lennard–Jones clusters. *J. Phys. Chem.* **91**(19), 4950 (1987).
36. B. Gludovatz, S. Wurster, A. Hoffmann, and R. Pippan: A study into the crack propagation resistance of pure tungsten. *Eng. Fract. Mech.* **100**, 76 (2013).
37. D. Hull, P. Beardmore, and A.P. Valintine: Crack propagation in single crystals of tungsten. *Philos. Mag.* **12**(119), 1021 (1965).
38. J.P. Hirth and J. Lothe: *Theory of Dislocations* (Wiley-Interscience Press, New York, 1982); p. 764.
39. K. Nishimura and N. Miyazaki: Molecular dynamics simulation of crack growth under cyclic loading. *Comput. Mater. Sci.* **31**, 269 (2014).
40. P. Wang, J.G. Xu, Y.G. Zhang, and H.Y. Song: Molecular dynamics simulation of effect of grain on mechanical properties of nano-polycrystal alpha-Fe. *Acta Phys. Sin.* **65**, 236201 (2016).
41. L. Yan and J.K. Fan: In situ SEM study of fatigue crack initiation and propagation behavior in 2524 aluminum alloy. *Mater. Des.* **110**, 592 (2016).

https://doi.org/10.1557/jmr.2017.114 Published online by Cambridge University Press